Energy and Buildings 153 (2017) 448–460

Contents lists available at ScienceDirect

Energy and Buildings

journal homepage: www.elsevier.com/locate/enbuild

Evaluating energy consumption saving from translucent concrete building envelope

Aashish Ahuja [a], Khalid M. Mosalam [b,*]

[a] Department of Mechanical Engineering, University of California, Berkeley, CA 94720, USA
[b] Department of Civil and Environmental Engineering, University of California, Berkeley, CA 94720, USA

ARTICLE INFO

Article history:
Received 16 February 2017
Received in revised form 6 May 2017
Accepted 20 June 2017

Keywords:
Daylighting
Energy utilization
Markov chain method
Solar radiation
TC panels
Thermal analysis

ABSTRACT

The translucent concrete (TC) as a building envelope can offset some lighting energy that is consumed within a room in an office. It is constructed from concrete panels which are functionalized by embedding optical fibers during the manufacturing phase to transmit sunlight. From preliminary results, a volumetric fiber ratio of 6% used in the TC panel leads to savings in lighting energy by around 50%. The utility of panels is enhanced if it reduces the heating and cooling requirements of the office room. The sunlight channeled by optical fibers can contribute in heating of room during winter but in summer months, it leads to spike in cooling loads. Also, daylight reduces heat dissipation from lighting installations and positively impacts cooling loads. The conduction through walls allows heat to be removed from the room during morning but transmits heat from ambient environment into the room later in the afternoon and evening. The presented research combines thermal and lighting analyses to search for an optimal fiber volumetric ratio for TC panels that would result in energy savings. The TC panels can cut down energy expenditure by 18% for a fiber volumetric ratio of 5.6% which renders the fabrication process to be practical.

1. Introduction

The utilization of sunlight to illuminate the interior spaces of buildings is beneficial as it provides the human occupants with a healthy environment. Moreover, it contributes to energy savings by decreasing the electricity used for artificial lighting. Currently, exterior glazing is the primary approach to allow natural daylight to pass through a building's façade. Also, we observe that the amount of external glazing used in a building, measured by window-to-wall ratio (WWR), is increasing in new and retrofitted buildings. A number of industry codes in the United States like *ASHRAE* 90.1-2010 and *ASHRAE* 189.1-2013 proposed to limit the amount of glazing citing low insulation value, high solar heat gains, and the potential for glare within the space. In addition, structural safety under extreme loading conditions mandates reducing glazing or structurally assessing and designing the glass curtain walls, which are traditionally viewed as non-structural components, refer to Lu et al. [14,15]. This paper considers replacing glazing by load-bearing panels that can be functionalized for light transmission, namely the translucent concrete (TC) panels.

Since the demand for natural daylighting inside the buildings is well established, building designers are beginning to seek means other than windows to capture, transport, and deliver natural light into the interior spaces of the building. A recent study on novel façade material made of organic material like sucrose and capable of diffusing light was published by Gutierrez and Zohdi [5]. Designers have also started using flexible solar light pipes for transmitting light into the inner rooms of the building. The interests in using alternative sources of lighting have led to the development of TC panels, which are envisioned to coexist with windows in a building so as to not restrict the occupant's view to the outside environment or hamper an architect's ability in designing aesthetically appealing buildings. As we see in Ahuja et al. [2], the optical fibers in the panel have the ability to reduce glare and save up to 50% lighting energy using a reasonable fiber volumetric ratio of ~6%.

The utility of TC panels is enhanced if it can also reduce the heating and cooling loads of the office room. The solar radiation, consisting of the entire spectrum of sunlight (ultraviolet, visible and infrared), channeled by optical fibers can contribute in heating the room during the winter season. On the other hand, if the optical fiber density in the TC panels is high, solar radiation leads to overheating and causes cooling loads to consume larger portion of the building energy. Moreover, the use of natural daylight in illuminating the office work space reduces heat dissipation from lighting installations and positively impacts cooling loads. Moreover, con-

* Corresponding author.
E-mail address: mosalam@berkeley.edu (K.M. Mosalam).

http://dx.doi.org/10.1016/j.enbuild.2017.06.062
0378-7788/

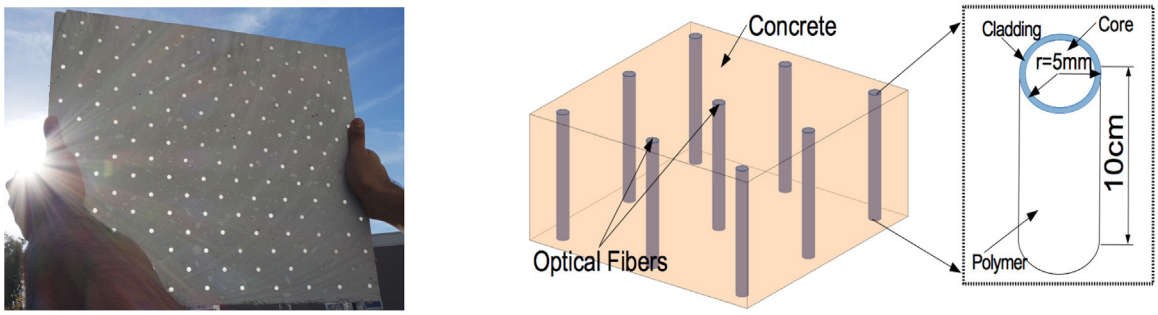

Fig. 1. (a) A TC panel manufactured in the laboratory held against the sun and transmitting light, and (b) a computational model of TC panel with embedded optical fibers (illustration not to scale).

duction through the walls allows heat to be removedfrom the room during the morning but transmits heat from the ambient environment into the room later in the afternoon and evening. A thermal analysis algorithm is developed to calculate the heat transfer due to solar radiation, conduction through walls and heat dissipation from lighting installations.The thermal analysis is coupled with lighting analysis to search for an optimal optical fibervolumetric ratio for the TC panels that would reduce the energy expenditure on lighting, heating and cooling with respect to energy spent in a daylight-deprived room with opaque walls.

Further advancements in this technology involve substituting normal weight concrete (NWC) with a new building material called the ultra-lightweight cement composites (ULCC) developed in Wu et al. [25]. The composite material achieves its light weight from the inclusion of cenospheres that coincidentally also enhances the thermal insulation of ULCC. The previously mentioned simulations are repeated by substituting NWC with ULCC and a small increase in overall energy saving is observed.

The TC panel has the potential to redefine the way people think of concrete walls, from that of opaque and bland element of the envelope, to one that is transporting and providing natural daylight into the interior space of an otherwise artificially lit room. Thus,it is envisioned that together with existing building components, the TC panels might be able to save energy and also offer a comfortable indoor environment to its occupants.

2. Theory and modeling

2.1. Constructing and modeling the TC panel

In the study, the TC is manufactured in the laboratory in the form of panels with dimensions 0.3 m × 0.3 m × 0.1 m. The same dimensions are used as reference in computational modeling of the TC panel. The manufactured unit of TC panel and its equivalent computational model are shown in Fig. 1. Each TC panel consists of optical fibers embedded during the construction of the concrete panel and by varying the volumetric ratio of these fibers, one can control the transparency of the panel. The optical fiber is a cylinder with diameter of 5 mm. The light travels in the core of the optical fiber which is made of PMMA (Poly-Methyl MethAcrylate). This core is surrounded by a thin layer of PF (PerFluorinated) polymer known as the cladding, which protects the core and allows light to propagate by Total Internal Reflection (TIR) at the core-cladding interface. The refractive index of the cladding is less than that of the core, a requirement necessary to initiate TIR. Also, in the case of plastic optical fibers, refractive indexes vary slightly over a range of wavelengths (280–4000 nm) as given in [7]. This study used a refractive index of 1.49 for the core and 1.40 for the cladding, which were provided by the manufacturer of the considered type of fiber with a numerical aperture (*N. A.*) ($= \sqrt{n_{core}^2 - n_{cladding}^2}$) of 0.51. The numerical aperture exhibits a limited acceptance cone for light transmission given in Fig. 2.

2.2. Transmission behavior of optical fibers

The optical fibers in the TC panel undergo three noticeable phenomena: reflection and refraction on its top surface and TIR along the inside walls of the fiber. The fraction of light energy refracted into the optical fiber medium is given as in Zohdi [26]:

$$\Re = 1 - \frac{1}{2}\left(\left(\frac{\frac{\hat{n}^2}{\hat{\mu}}\cos\theta_i - \sqrt{\hat{n}^2 - \sin^2\theta_i}}{\frac{\hat{n}^2}{\hat{\mu}}\cos\theta_i + \sqrt{\hat{n}^2 - \sin^2\theta_i}}\right)^2 + \left(\frac{\cos\theta_i - \frac{1}{\hat{\mu}}\sqrt{\hat{n}^2 - \sin^2\theta_i}}{\cos\theta_i + \frac{1}{\hat{\mu}}\sqrt{\hat{n}^2 - \sin^2\theta_i}}\right)^2\right) \quad (1)$$

where $0 \le \Re \le 1$ for an angle of incidence θ_i, $\hat{\mu} = \mu_t/\mu_i = 1$ ($\hat{\mu}$ is the ratio of magnetic permeabilities for transmission and incident media) and $\hat{n} = n_t/n_i$ ($\hat{n}$ is the ratio of refractive indices for transmission and incident media). Light rays that do not follow the TIR are converted to heat within the fiber.

2.3. Ray tracing and light losses in optical fibers

The interaction of light rays with optical fibers is computed using a ray tracing method. The development of the ray tracing solver used in this research has been described in detail in Ahuja et al. [1]

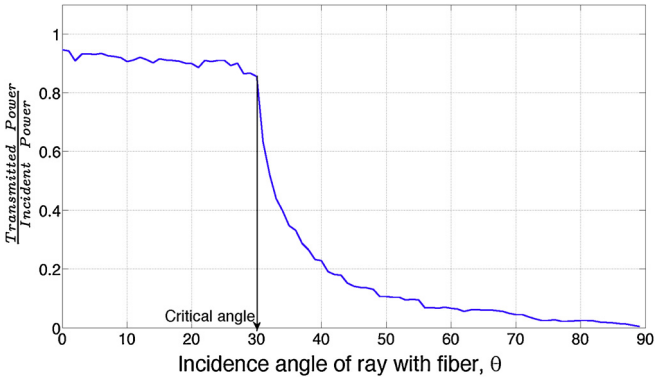

Fig. 2. Performance of optical fiber deteriorates as light rays subtend larger angles with fiber. All meridonial rays intersect the centerline of the fiber during ray tracing.

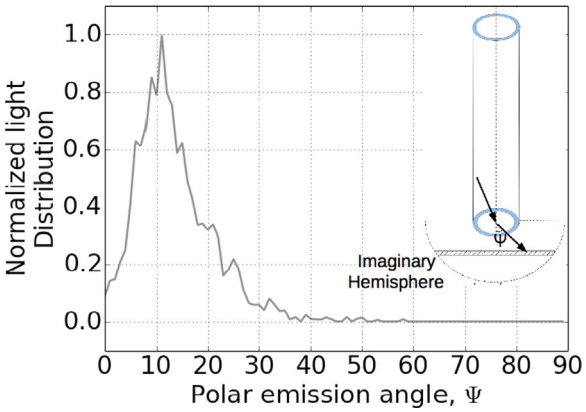

Fig. 3. Normalized light distribution exiting from the fiber into the room at different polar emission angles, Ψ. The largest fraction of light flux is transmitted along $\Psi = 11^{\circ}$.

and Zohdi [26]. The theory for ray tracing and its complete trajectory discretization in space for advancing light rays using numerical techniques is detailed in Appendix A. Ray tracing proceeds by tracking each ray in the core of the optical fiber as it changes trajectory. The solver also accounts for intrinsic losses of light occurring within the fiber according to Zubia and Arrue [27]. These losses include:

1 Rayleigh scattering in the fiber from the random density fluctuations caused by irregular microscopic structure of the fiber. For a PMMA core, the loss factor is $\alpha_R = 13 \times \left(\frac{633}{\lambda}\right)^4$ dB/km [8].
2 Light absorption from electronic transitions between the excited and the ground state. Loss factor is $\alpha_e = 1.58 \times 10^{-12} \exp\left(\frac{1.15\times10^4}{\lambda}\right)$ dB/km [9].

Light absorption leads to heating up of the optical fiber, whereas the radiation dissipated via the scattering process is rejected from the optical fiber. The significant terrestrial radiation (280–4000 nm) is broken into 3 spectra: Ultraviolet (UV) range (280–380 nm), visible light range (380–780 nm) and infrared (IR) range (780–4000 nm) of solar radiation. The intrinsic transmittance of a PMMA optical fiber with rays having an average optical path length of L (in km) is calculated by applying Eq. (2) as given in [10] to each spectrum of terrestrial radiation.

$$T(L) = \frac{\int_{\lambda_1}^{\lambda_2} E_o(\lambda) \exp(-(\alpha_R + \alpha_e)L) d\lambda}{\int_{\lambda_1}^{\lambda_2} E_o(\lambda) d\lambda} \quad (2)$$

where the solar spectral distribution, $E_o(\lambda)$ as a function of the wavelength λ, is defined as $E_o(\lambda) = \frac{C_1}{\lambda^5[\exp(C_2/\lambda)-1]}$ with $C_1 = 8.097 \times 10^{-21}$ Wm^2 and $C_2 = 2.497 \times 10^{-6}$ m. Eq. (2) is applied to calculate the attenuation in the intensity of each ray as a function of the length travelled by the ray in an attenuating medium like optical fiber.

2.4. Computing savings in lighting energy

The savings in lighting energy from TC panels is calculated using the procedure described in Ahuja et al. [2]. The procedure is summarized in the following paragraphs.

2.4.1. Choosing a sky model

The ray tracing algorithm for a TC panel is coupled with a solar radiation model to estimate the amount of sunlight that is transmitted by the panel. The Perez-sky Model [19] extracts hourly data for sunlight irradiances/illuminances from the typical meteorological year (TMY) weather file for a location and differentiates the values into their components (direct radiation, isotropic radiation, circumsolar disk radiation and horizon brightening). The equations for Perez-sky model are modified further to calculate the transmission of radiation by TC panels and used in this research.

2.4.2. Illumination calculations over a workplane

The calculations for the illumination of a workplane due to transmission of light by the TC panels was executed in the far field where the crossing of rays (caustics) is negligible and the illumination distribution has the form of the intensity distribution. The optical fiber has a circular end and hence, the far field is defined as the region outside an imaginary hemisphere with a radius bigger than at least five times the diameter [12]. The *RADIANCE* software can model customized luminaires and define the luminous intensity distribution, using the function *ies2rad*, for calculating illuminance at different points inside the modeled room. The optical fiber is a point source that emits diffused light according to the transmission curve illustrated in Fig. 3, calculated using

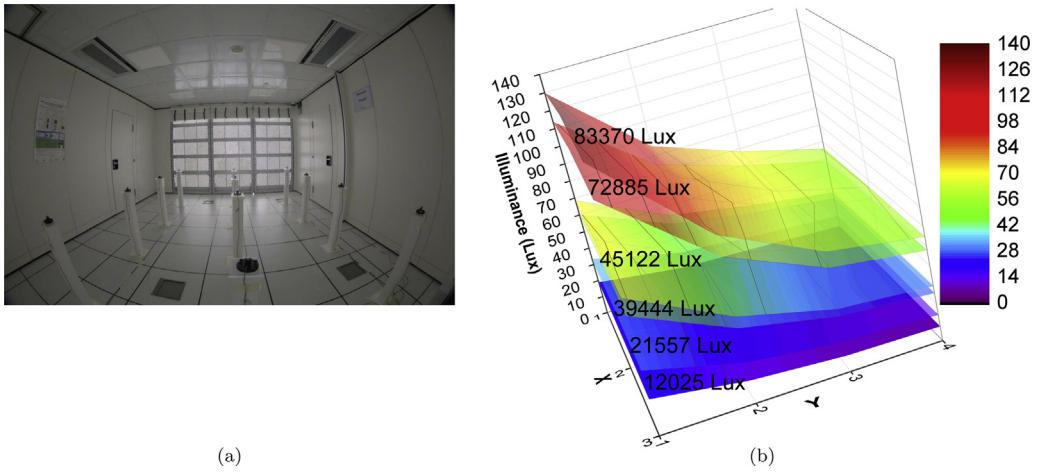

(a) (b)

Fig. 4. (a) Interior HDR photograph of testbed room, and (b) distribution of measured indoor illuminance at different emulated light intensities.

ray tracing. The average luminous intensity, $I_{c(\Delta\omega_i)}$, emitted into a solid angle, $\Delta\omega_i$ is expressed as:

$$I_{c(\Delta\omega_i)} = \frac{\Delta\Phi_i}{\Delta\omega_i} = \frac{v_i\Phi}{\Delta\omega_i\sum_{i=0}^{89} v_i} \tag{3}$$

where $\Delta\Phi_i$ is the light flux passing through $\Delta\omega_i$, v_i takes a value between $0 \le v_i \le 1$ and normalizes the proportion of light associated with $\Delta\omega_i$ with respect to the light flux passing through $\Delta\omega_{11}$ (the maximum light flux passes through $\Delta\omega_{11}$ as observed in Fig. 3). Φ is the net light flux emitted by the exit aperture of the optical fiber which is distributed between 90 elevation angles of 1° each, that cover the entire hemisphere. Each $\Delta\omega_i$ is a three dimensional angle subtended by a section of the hemisphere that can be represented as:

$$\Delta\omega_i = 2\pi(\cos i - \cos(i+1)) \tag{4}$$

where $0 \le i \le 89$.

2.4.3. Preliminary experimental results

The TC panels in Fig. 1a were used to create a wall in the experimental testbed setup that allows full-scale experimentation. The TC wall was excited using a daylight emulator and the illuminance (in *lux*) was calculated at the 12 sensors that occupy the room as shown in Fig. 4a. The results for distribution of indoor illuminances at different light intensity excitations are shown in Fig. 4b. We observe from Fig. 4b that the optical fibers emit diffused light such that all sensors placed at equal *y*-distance from the wall records almost similar illuminance values. This is also observed from simulations and thus, qualitatively, compares well with preliminary experimental results.

Remark: In the future, the testbed containing TC panels will be simulated and the computed results for illuminances will be compared with sensor recorded values.

2.4.4. Occupancy estimation:

A randomized model for occupancy, called the inhomogeneous Markov chain Monte Carlo method [18] was applied to real occupancy data acquired from an office room with three occupants, situated in Cory Hall, UC Berkeley, to predict the lighting requirements of the room. The Markov chain model for occupancy uses the idea that the probability of presence at a time step only depends on the state of presence at the previous time step. In other words, the probability that an occupant is present now only depends on whether he/she was present one time step ago and not on whether he/she has been present over a past long period of time. The situation is described using two parameters: (i) the profile of probability of presence of occupants over a typical week and (ii) a parameter of mobility that gives an idea of how frequently people move in and out of their office zone. These parameters are then used to capture the time-dependent probabilities of transitions, T_{ij}, for each occupant as they switch between states of presence and absence. The algorithm for calculating occupancy is represented as a flow chart in Fig. 5.

2.4.5. Light switching predictions

The current research includes three kinds of light switching activities that are commonly observed in offices and commercial buildings. These are:

1 Switch-on at arrival
2 Intermediate switch-on
3 Intermediate switch-off

The use of manual controls by the user are tied to their presence in the room. For this, we use multiple models that simulate

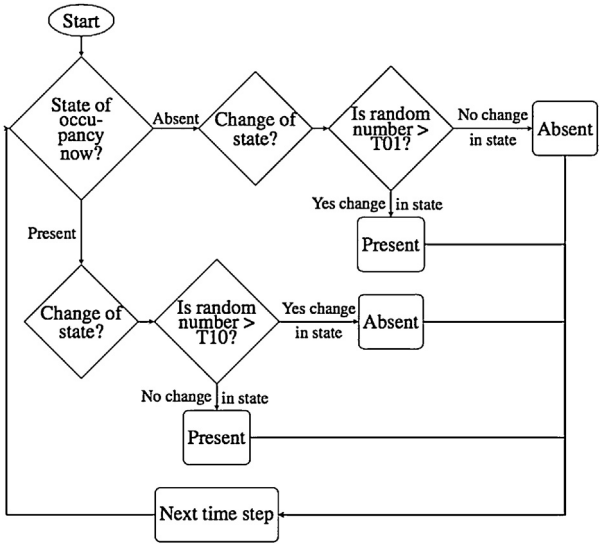

Fig. 5. Occupancy model algorithm proposed by Page et al. [18] and used in this study.

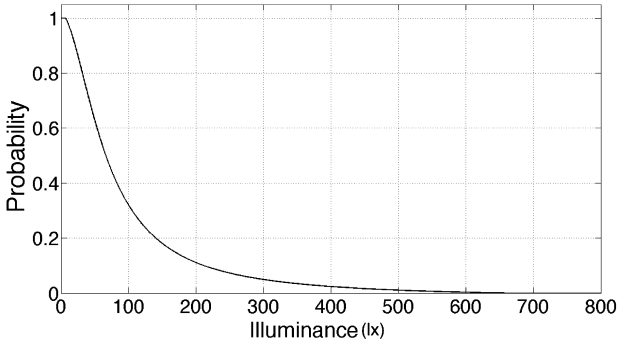

Fig. 6. Probabilistic curve for switch-on at arrival.

the switching actions of users for different events. The probabilistic curve for switch-on at arrival was adapted from Hunt [6], which was developed using time-lapse photography to emulate the occupants switch-on action at arrival in the room. It is also observed that the users seldom operate switches while they have been present for sometime in the room. This curve, shown in Fig. 6 relates the amount of desk illuminance to the likelihood of an occupant switching on the light.

The intermediate light switching means the act of interacting with artificial lighting at occasions other than upon arrival to or before departure from the office. The intermediate switching-on event was shown to be dependent on the illuminance threshold of the users Lindelöf and Morel [11]. As soon as the illuminance reduced below the threshold, the switch-on probability sharply rose to a level between 1% and 4%. The data for intermediate switch-on probability is presented in Fig. 8. The probability of an intermediate switching-off event is observed to be much lower than an intermediate switching-on event as shown in Fig. 7. This indicates that the users switched off their lights mostly on their way out of the office while keeping the lights switched on for the rest of the day. For all the light-switching models, it is argued that the occupants' actions are a function of the minimum illuminance received on the workplane. This observation has been demonstrated in Reinhart and Voss [23], Love [13], Boyce et al. [3], Pigg et al. [20].

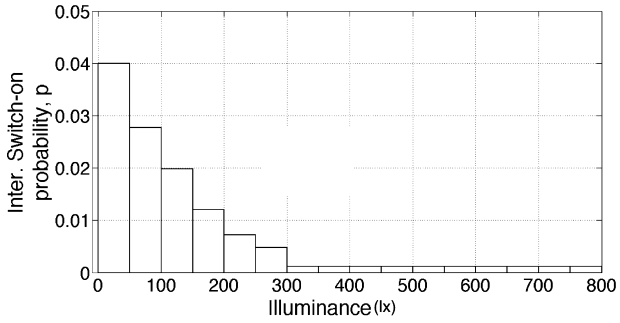

Fig. 7. Intermediate switch-on (for illuminance = 0, $p = 1.0$ is assumed).

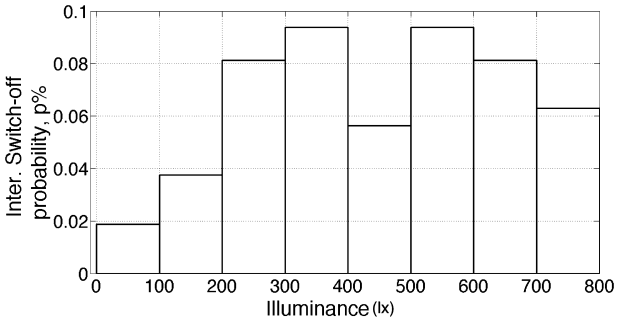

Fig. 8. Intermediate switch-off (for illuminance = 0, $p = 1.0$ is assumed).

2.4.6. Pseudo code and assumptions

The pseudo code for energy savings estimator is presented in Algorithm 1. The algorithm begins with the precondition that illuminance on the workplane for each occupant is available. Using Markov chain model, the algorithm generates a randomized annual occupancy profile. The switching models based on illuminance values and the occupancy status (*i. e*. Present or Absent) at the current moment decides whether the user prefers artificial lighting or sunlight. Total energy savings is simply the energy offset (in kWh) during the year when the occupant did not use electric lighting.The switch-off probability at departure was excluded from the lighting performance model. It was assumed that the lights had occupancy sensors which switched off automatically as soon as the occupants left their space. Luminaire Rating is the power consumed by electrical lighting to illuminate the desk of an occupant. The procedure given in Algorithm 1 is averaged over 100 profiles to give a mean prediction of energy savings.

Algorithm 1. Energy savings estimator

Require Ray Tracing using ~ 100,000 rays: *Calculate* Φ
Require Workplane illuminance to be calculated
save ⟵ 0
for 1 to 100 **do**
  Generate: Annual Occupancy Profile
  for (1 to 365 days) **do**
    switch ⟵ 0
    occ_{i-1} (at 8 am) ⟵0
    T = 8 am
    while (*T* < 6 pm) **do**
      illum ⟵ *Workplane Illuminance*
      occ_i ⟵ *CurrentOccupancy*
      if occ_{i-1} and occ_i is 0 **then**
        switch ⟵ 0
      else if occ_i is 1 **then**
        if occ_{i-1} is 0 **then**
          switch ⟵ *SwitchOnAtArrival*
          if *switch* is 0 **then**
            save++
        else ifocc_{i-1} is 1 and *switch* is 1 **then**
          switch ⟵ *SwitchOnInter*
          if*switch* is 0 **then**
            save++
        else
          switch ⟵ *SwitchOffInter*
          if *switch* is 0 **then**
            save++
      T +=1/2 h (Energy savings are calculated every half-hour)
  Savings per occupant is calculated as:
  $LuminaireRating \times save/100(kW) \times 1/2(hr)$

2.5. Heat conduction in TC panels

The TC panel consists of concrete and plastic optical fibers that are both known to conduct heat when exposed to a temperature difference. The optical fibers, moreover, channel heat and radiate it into the room. They use the same principles for heat radiation as were used to transmit light (see Section 2.2). The total heat that enters/leaves the room increases the loads on the HVAC (heating, ventilation and air-conditioning) system which are important in estimating its sizing.

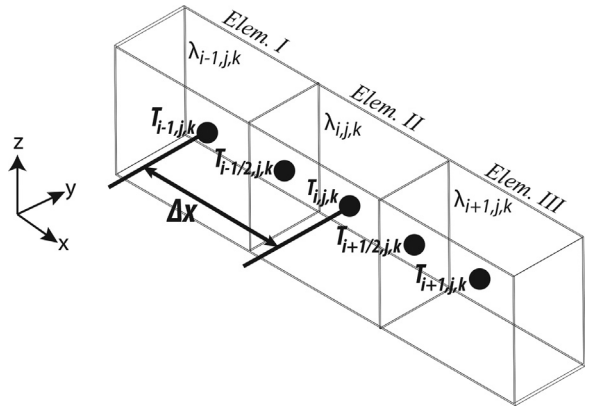

Fig. 9. Elements, *I*, *II* and *III*, with different material properties. Intermediate grid points $T_{i+1/2,j,k}$ and $T_{i-1/2,j,k}$ between elements, *I* & *II* and *II* & *III*, respectively.

2.5.1. Finite difference method for conduction

The general heat transfer in a multi-layered wall due to conduction of heat is given as follows:

$$\rho c_p \frac{\partial T}{\partial t} = \nabla.(\boldsymbol{\lambda} \nabla T) \tag{5}$$

where $\rho = \rho(\vec{r})$ is the mass density of the TC panel, $c_p = c_p(\vec{r})$ is the specific heat at constant pressure and $\boldsymbol{\lambda} = \boldsymbol{\lambda}(\vec{r})$ is the heat conductivity of the TC which are dependent on location, $\vec{r} = (x, y, z)$.

To solve Eq. (5) numerically, a 3D finite difference scheme based on explicit discretization of the heat equation and supporting inclusion of heterogeneous materials as given in Praprotnik et al. [21] was adopted. The code was validated in Praprotnik et al. [21] by solving the heat conduction equation, analytically and numerically using the presented scheme, on a 1-D heat conductor composed of two materials with the same thicknesses but different densities, specific heats and conductivity constants. The convergence criteria for the validation problem was set as $T^{n+1}_{k-1} - T^{n}_{k-1} < \epsilon = 10^{-15}$ (where *T* is the temperature, *k* is the node number and n is the current time step). The validation study given in the reference was conducted using Python platform prior to solving the transient heat transfer problem in current research. The properties of heterogeneous materials (*i. e*. concrete, XPS and drywall) used in the construction of a multilayered wall can be easily accounted for in this scheme. A special mesh is generated to cover the volume of the domain. First, grid nodes are placed at the center of grid elements as shown in Fig. 9. Then, to fulfil the transient condition for equality of temperature at the interfaces between grid elements, new intermediate grid points are introduced ($T_{i+1/2,j,k}$, $T_{i-1/2,j,k}$ along the

x axis; similar points are added along y and z axes) on the interface between grid elements as labeled in Fig. 9. Within each grid element the properties are homogeneous (*i. e.* $\boldsymbol{\lambda} = \lambda \mathbf{I}$) such that the second spatial derivative of temperature at the center of a 3D grid element is given as:

$$\rho c_p \frac{\partial T}{\partial t} = \lambda \left(\frac{\partial^2 T}{\partial x^2} + \frac{\partial^2 T}{\partial y^2} + \frac{\partial^2 T}{\partial z^2} \right) + \frac{\partial \lambda}{\partial x} \cdot \frac{\partial T}{\partial x} + \frac{\partial \lambda}{\partial y} \cdot \frac{\partial T}{\partial y} + \frac{\partial \lambda}{\partial z} \cdot \frac{\partial T}{\partial z} \tag{6}$$

The value of λ is constant within a grid element, *i. e.* $\frac{\partial \lambda}{\partial x} = \frac{\partial \lambda}{\partial y} = \frac{\partial \lambda}{\partial z} = 0$. Therefore, the discretization of Eq. (6) in time, t, and space, x, y, z gives:

$$\rho_{i,j,k} c_{p_{i,j,k}} \frac{T^{n+1}_{i,j,k} - T^{n}_{i,j,k}}{\Delta t} = 2\lambda_{i,j,k} \left(\frac{T^{n}_{i+1/2,j,k} - 2T^{n}_{i,j,k} + T^{n}_{i-1/2,j,k}}{\Delta x^2} + \frac{T^{n}_{i,j+1/2,k} - 2T^{n}_{i,j,k} + T^{n}_{i,j-1/2,k}}{\Delta y^2} + \frac{T^{n}_{i,j,k+1/2} - 2T^{n}_{i,j,k} + T^{n}_{i,j,k-1/2}}{\Delta z^2} \right) \tag{7}$$

Indices $\{i, j, k\}$ denote the spatial discretization in the $\{x, y, z\}$ directions, respectively, and Δx, Δy, Δz are the corresponding spatial step sizes. The time discretization is implied by the superscripts in terms of n with time step being Δt.

At the interface of grid elements with different material properties, the flux conservation condition holds:

$$\lambda_{i,j,k} \frac{\partial T}{\partial x}\bigg| i, j, k = \lambda_{i+1,j,k} \frac{\partial T}{\partial x}\bigg| i+1, j, k \tag{8}$$

$$\lambda_{i-1,j,k} \frac{\partial T}{\partial x}\bigg| i-1, j, k = \lambda_{i,j,k} \frac{\partial T}{\partial x}\bigg| i, j, k \tag{9}$$

The 3D interface conditions given in Eqs. (8) and (9) are discretized and rearranged as follows:

$$T_{i\pm1/2,j,k} = \frac{\lambda_{i,j,k} T_{i,j,k} + \lambda_{i\pm1,j,k} T_{i\pm1,j,k}}{\lambda_{i,j,k} + \lambda_{i\pm1,j,k}} \tag{10}$$

$T_{i,j\pm1/2,k}$ and $T_{i,j,k\pm1/2}$ are defined similarly to Eq. (10). The heat equation for the TC panel also considers the heat dissipated inside the fiber smeared evenly along the entire length of the fiber. To represent the effect of heat dissipation in fiber, the following heat equation has been introduced to supplement Eq. (5):

$$\rho c_p \frac{\partial T}{\partial t} = \nabla . (\boldsymbol{\lambda} \nabla T) + q_{dis} \tag{11}$$

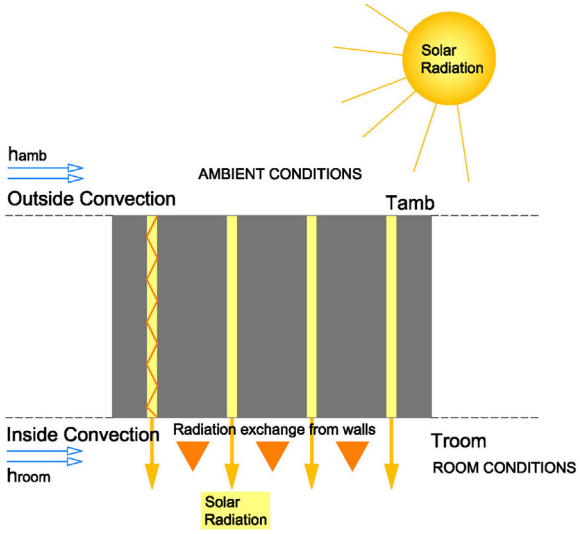

Fig. 10. Heat exchange between TC panel, outside ambient and indoor room conditions. Illustrative image of a section of the TC panel and modes of heat transfer.

where q_{dis} is the heat dissipated in fiber of RVE. For each element, the discretization in Eq. (7) is rewritten as:

$$\rho_{i,j,k} c_{p_{i,j,k}} \frac{T^{n+1}_{i,j,k} - T^{n}_{i,j,k}}{\Delta t} = 2\lambda_{i,j,k} \left(T^{n}_{i+1/2,j,k} - 2T^{n}_{i,j,k} + \frac{T^{n}_{i-1/2,j,k}}{\Delta x^2} + \frac{T^{n}_{i,j+1/2,k} - 2T^{n}_{i,j,k} + T^{n}_{i,j-1/2,k}}{\Delta y^2} + \frac{T^{n}_{i,j,k+1/2} - 2T^{n}_{i,j,k} + T^{n}_{i,j,k-1/2}}{\Delta z^2} \right) + (q_{dis})_{i,j,k} \tag{12}$$

Interface Eqs. (8) and (9) holds in this case as well.

2.6. Boundary conditions and assumptions

The heat transfer mechanisms for a TC panel consists of (1) Heat conduction through both the concrete and optical fibers, (2) Convection of heat from TC exterior and interior-facing surfaces to ambient environment and room, respectively, (3) Radiation to sky and walls of the room, (4) Light absorption in optical fibers [9] and later dissipation in form of heat, (5) Direct and diffuse solar radiation transmission by optical fibers into the interior of the room. This leads to rise in the temperature of the TC panel during the day and also transfer some of that heat due to conduction and radiation. The scenario of thermal exchange between the TC panel, the ambient environment and indoors is represented in Fig. 10.

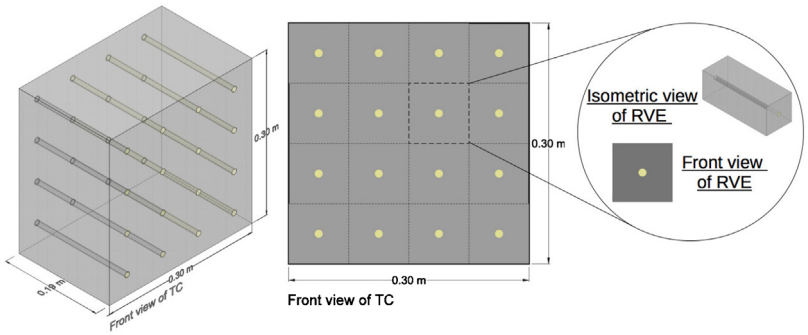

Fig. 11. RVE of a TC panel with 4 × 4 fibers arranged in a regular pattern.

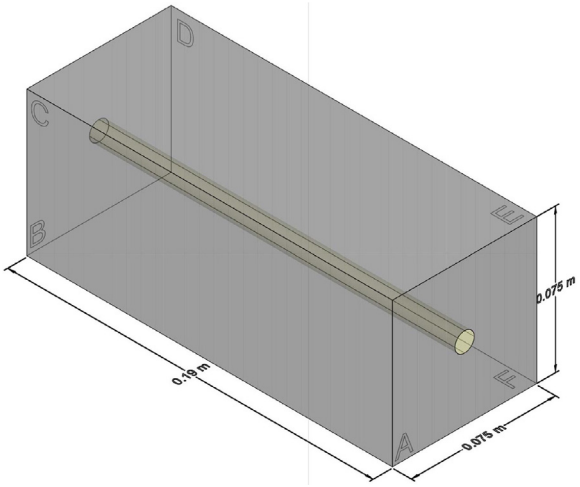

Fig. 12. Isometric view of the RVE. The faces of RVE are named from A to F.

The TC panel can be divided into a number of smaller 'Representative Volume Elements (RVEs)' such that each element preserves the volumetric ratio of fibers as was modeled in the original TC panel composite. An example of a RVE in a TC panel containing 16 fibers (arranged in a 4×4 pattern) is shown in Fig. 11. The RVE in the figure is a single volume that consists of only one fiber such that each TC panel is composed of 16 RVEs. An isometric view of a RVE is given in Fig. 12. The mesh for RVE is given in Fig. 13. The different colors along the length of RVE represents the different layers of the wall (concrete, XPS insulation, drywall) while the mesh in center of the block is used to discretize the fiber. The faces are marked as *A*, *B*, *C*, *D*, *E* and *F*. The following boundary conditions are applied:

1 Faces *C* through *F* of a RVE from TC panel are surrounded by other similar RVEs and thus, we can apply periodic boundary conditions (PBCs) to RVE. PBCs are defined as conditions which are chosen for approximating or simulating a large system by using a small part called a unit cell or RVE. The solution at the RVE faces $C - F$ are periodic as a function of each of the spatial variables. Therefore, in the heat transfer problem the following PBCs are applied:
(a) The temperature at both ends is equal

$$T(0, y, z, t) = T(W, y, z, t); \quad T(x, 0, z, t) = T(x, H, z, t) \tag{13}$$

where W is the width and H is the height of the panel.

(b) The heat flux at both ends is equal

$$\frac{\partial T}{\partial x}(0, y, z, t) = \frac{\partial T}{\partial x}(W, y, z, t); \frac{\partial T}{\partial y}(x, 0, z, t) = \frac{\partial T}{\partial y}(x, H, z, t) \tag{14}$$

Remark: It is assumed that the same RVE blocks are repeated several times to create a south-facing TC wall. The connections between the TC panel edges are not taken into account as that would have required meshing an entire TC panel containing several fibers which would have significantly raised the computational cost. Using supercomputing capabilities and same algorithm, it is possible to re-design and simulate the current heat transfer problem such that it contains thermal bridges and connections between TC panels. Currently, it is outside the scope of our research.

2 Face *A* overlooks the interior of the room. It is exposed to the room air and also has radiation exchange with the rest of the surfaces inside the room. It is assumed that face *A* is surrounded by surfaces (other walls, ceiling, floor) that act like a hemispherical cap around the wall surface and subtends a half angle of 90° which results in a view factor of $F_{12} = \sin^2 90° = 1$. The view factor F_{12} is the fraction of energy exiting an isothermal surface 1 by emission, that directly impinges and is absorbed on surface 2. View factors depend only on geometry. The RVE exchanges radiation with room at mean radiant temperature, T_{mean}, which is calculated from the weighted average of the surface temperatures for the three walls, *i. e*. those without TC panels, ceiling and roof adjacent and opposite to the wall containing TC panels. The heat balance across face *A* for both materials, concrete and fiber, can be represented as follows:

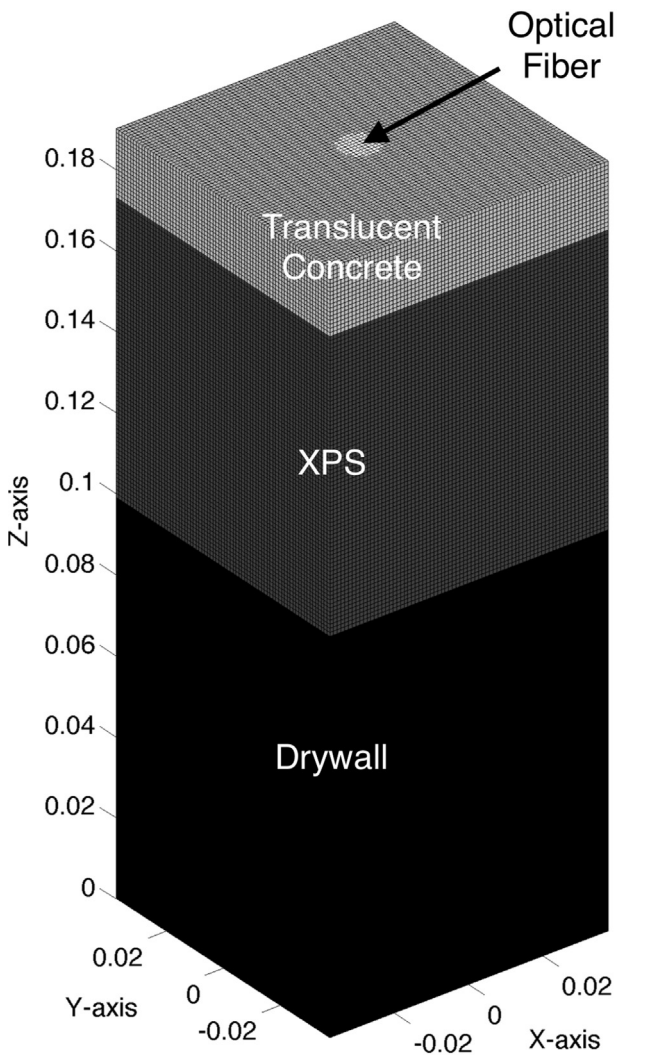

Fig. 13. Grid used for discretization of RVE. Different colors represent the layers of wall and fiber. The mesh size is $76 \times 76 \times 190$ elements. (For interpretation of the references to color in this figure legend, the reader is referred to the web version of the article.)

$$-\lambda \frac{\partial T}{\partial z}|_{FaceA} + h_{room}(T_{room} - T_A) + \epsilon\sigma(T_{mean}^4 - T_A^4) = 0 \tag{15}$$

where $T_A = T_A(x, y)$ is the temperature of face *A* of the RVE, h_{room} is the convection coefficient inside the room with set-point temperature for cooling and heating given as T_{room}, $\epsilon = 0.95$ is the emissivity of all the surfaces inside the room and $\sigma = 5.6703 \times 10^{-8}$ W/(K^{4}m^2) is the Stefan–Boltzmann constant. The discretized form of Eq. (15)

which is valid for both, fiber and concrete, constituting face A is expressed as follows:

$$\epsilon\sigma(T_{mean}^4 - T_{i,j,k+1/2}^4) + h_{room}(T_{room} - T_{i,j,k+1/2}) - \frac{2\lambda_{i,j,k}}{\Delta z}(T_{i,j,k+1/2} - T_{i,j,k}) = 0 \quad (16)$$

The terms are rearranged to give Eq. (17) which is solved for $T_{i,j,k}$ making use of Eq. (10) written for $T_{i,j,k+1/2}$ instead of $T_{i\pm1/2,j,k}$ using Newton's iterations.

$$\epsilon\sigma T_{i,j,k+1/2}^4 + \left(h_{room} + \frac{2\lambda_{i,j,k}}{\Delta z}\right) T_{i,j,k+1/2} + \left(-\frac{2\lambda_{i,j,k}}{\Delta z} T_{i,j,k} - h_{room} T_{room} - \epsilon\sigma T_{mean}^4\right) = 0 \quad (17)$$

The total solar radiation (direct and diffuse), q_{sun}, is channeled through an optical fiber and transmitted directly into the room from face A which, acts as a sink and absorbs heat.

3 Face B interacts with the ambient environment. The concrete part of Face B absorbs solar radiation in the form of direct and diffused sunlight while the entire face exchanges heat with the surroundings using convection and radiation. The heat exchange for face B is given as:

$$\lambda \frac{\partial T}{\partial z}|_{FaceB} + h_{amb}(T_{amb} - T_B) + q_{solar} - \epsilon\sigma T_B^4 = 0, \text{ for concrete} \quad (18)$$

$$\lambda \frac{\partial T}{\partial z}|_{FaceB} + h_{amb}(T_{amb} - T_B) - \epsilon\sigma T_B^4 = 0, \text{ for fibers} \quad (19)$$

where $T_B = T_B(x, y)$ is the temperature of face B of the RVE, h_{amb} is the ambient convection coefficient, ϵ is emissivity (= 0.95) and q_{solar} is the solar radiation absorbed by the concrete part of face B. The concrete part of the TC panel is assumed to be leadership in energy and environmental design (LEED) certified, which sets its surface absorptivity value to throughout the solar spectrum [1]. Thus, only 36% of the total incident solar radiation is absorbed by concrete (q_{solar}) while 64% of incident solar radiation is reflected. Since the optical fiber guides solar radiation, the heat, q_{solar}, is not absorbed by the face of the fiber. In the discretized form, Eq. (18) can be written as follows:

$$\frac{2\lambda_{i,j,k}}{\Delta z}(T_{i,j,k-1/2} - T_{i,j,k}) + h_{amb}(T_{i,j,k-1/2} - T_{amb}) - q_{solar} + \epsilon\sigma T_{i,j,k-1/2}^4 = 0 \quad (20)$$

Eq. (19) can be discretized similarly. Rearranging the terms in the discretized forms for the concrete and optical fiber parts of face B gives:

$$\left(\frac{2\lambda_{i,j,k}}{\Delta z} + h_{amb}\right) T_{i,j,k-1/2} + \epsilon\sigma T_{i,j,k-1/2}^4 = \begin{cases} q_{solar} + h_{amb} T_{amb} + \frac{2\lambda_{i,j,k}}{\Delta z} T_{i,j,k} & \text{for concrete} \\ \frac{2\lambda_{i,j,k}}{\Delta z} T_{i,j,k} + h_{amb} T_{amb} & \text{for fiber} \end{cases} \quad (21)$$

The equations are solved using Newton's iterative solver.

4 Some limitations exist in the current model with respect to calculating the radiative heat exchange with exterior surroundings (*e. g.* ground and other buildings). Though the contribution of these quantities to the net heat transfer is small, their calculations would require complicated formulations which are better dealt by softwares like *EnergyPlus* (v8.5 Department of Energy (*DOE*), USA) and *Modelica* (v3.0, Lawrence Berkeley National Laboratory (*LBNL*), USA).

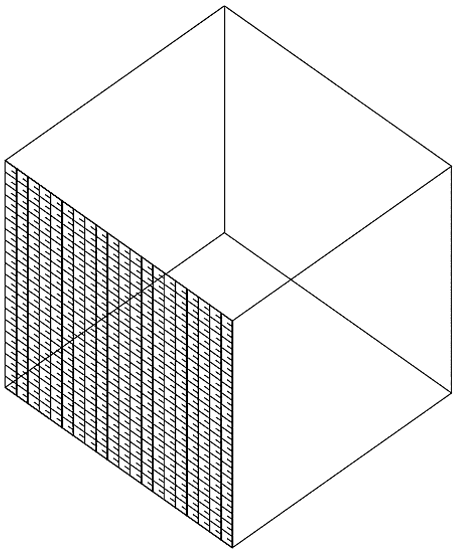

Fig. 14. Room model for conducting coupled thermal and lighting analyses in Berkeley.

3. Observations and discussion

The TC panel is exposed to heat due to the solar radiation incident on the wall and the temperature difference that exists between the outdoor environment and the indoor conditions. This leads to a rise in the temperature of the TC panel during the day and also transfers some of that heat into the room due to convection and radiation. The scenario of thermal exchange between the TC panel, the ambient environment and indoors for a place like Berkeley (California) was presented in Fig. 10.

3.1. Heat sources in the room

A model room (shown in Fig. 14) with a width and height of 3 m and a depth of 2.895 m is prepared for analyzing the impact of heat and light on the HVAC loads of the room. The room is maintained at 22 °C which corresponds to the set-point temperature for heating and cooling. The south-facing wall (shown with a checkered face in Fig. 14) is composed fully of TC panels. The heat, q_{sun}, arrives as diffused solar radiation into the space of the room through optical fibers in the TC panels. It is assumed that the solar radiation is instantly removed by the HVAC in the room to maintain the set-point temperature and hence, does not heat the walls of the room. Heat is also conducted into/out of the space through the walls of the room. The ceiling and floor of the room are insulated so there is no heat transfer through them. The room consists of three installations of T8 Fluorescent lamps consuming 32 W each. The lamps are designed to provide a constant illumination of 400 lx on workspaces of occupants. These lamps also dissipate 77% of their total input power as heat into the room during times of operation [22], which can further add to the cooling load of the HVAC system. Hence, it is important to control the daylight through the optical fibers in TC panels to provide sufficient illumination inside the room while also cutting back on the heat gains.

Remark 1. The set-point temperature of 22 °C was used since it corresponded to the temperature at which the highest occupant productivity was observed by Seppänen et al. [24].

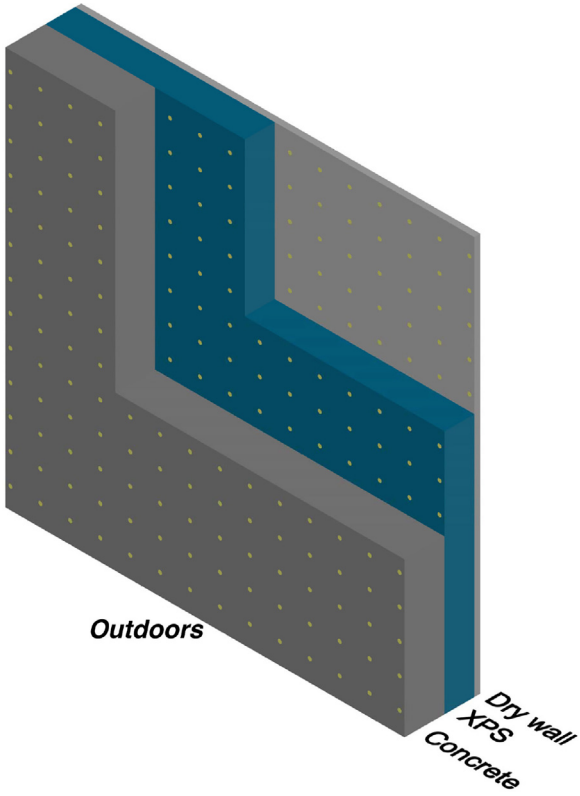

Fig. 15. The arrangement of different layers (concrete, Extruded PolyStyrene (XPS) insulation, drywall) in the walls of the room.

3.2. Parameters of heat conduction through walls

The walls facing North, East and West are opaque while the wall facing South are either translucent (with TC panels) or opaque (windowless). All the walls (including the wall with TC panels) are multi-layered and the layers are arranged as given in Fig. 15. The heat from ambient environment and solar radiation is conducted through the different layers of the wall including walls with TC panels. This heat is released into the room through the surfaces of walls facing the inside of the room. A fraction of this heat from a wall surface is convected into the room due to presence of HVAC circulated air while remaining heat is radiated and exchanged with the surrounding wall surfaces. The interior space considered here is small but the algorithm is modular to consider modifications in the room due to (1) geometry *i. e*. variations in room sizes (or wall and floor area dimensions) and thicknesses of walls, (2) material composition of walls, (3) number of occupants and (4) number of lighting installations. The geometrical dimensions and material properties for the layers in the walls and the heat transfer coefficients used in the simulations are listed in Table 1.

3.3. Total energy consumption from thermal and lighting analyses

Thermal and lighting simulations are conducted for the room shown in Fig. 14. The finite difference scheme presented previously is used to solve for heat conduction under appropriate boundary conditions. The heat conduction in opaque walls is calculated using a 1D model since the material properties are considered to be homogeneous in the plane of the wall, while for a TC panel, a 3D model of its RVE is used (Fig. 12). The occupancy models are used in conjunction with the light switching models to estimate the heat dissipated inside the room during the year due to the use of artificial lighting.

Table 1
Material properties and heat transfer coefficients for conduction.

Parameter	Value/expression
External walls	Concrete (0.1 m), XPS insulation (0.075 m), Drywall (0.0156 m)
Concrete mix composition	Water, cement, fly-ash, fine aggregate
R-value of layered-wall	2.81 m^2 K/W
R-value of fibers	1 m^2 K/W
$\lambda_{concrete}$	1.36 W/mK (Experimental results from SERIS, Singapore)
λ_{XPS}	0.028 W/mK
$\lambda_{drywall}$	0.276 W/mK, [16]
λ_{fiber}	0.2 W/mK
$\rho_{concrete}$	2180.79 kg/m^3 (Experimental results from SERIS, Singapore)
ρ_{XPS}	25 kg/m^3
$\rho_{drywall}$	752 kg/m^3, [16]
ρ_{fiber}	1180 kg/m^3
$c_{p,concrete}$	750 J/kgK
$c_{p,XPS}$	1500 J/kgK
$c_{p,drywall}$	1017 J/kgK, [16]
$c_{p,fiber}$	1450 J/kgK
h_{amb}	5.7 + 3.8 v_s W/m^2 K (v_s is outside wind speed, [17])
h_{room}	8.29 W/m^2 K (Recommended by *ASHRAE*)
Emissivity, ϵ	0.95
HVAC operating schedule	8 am to 6 pm daily

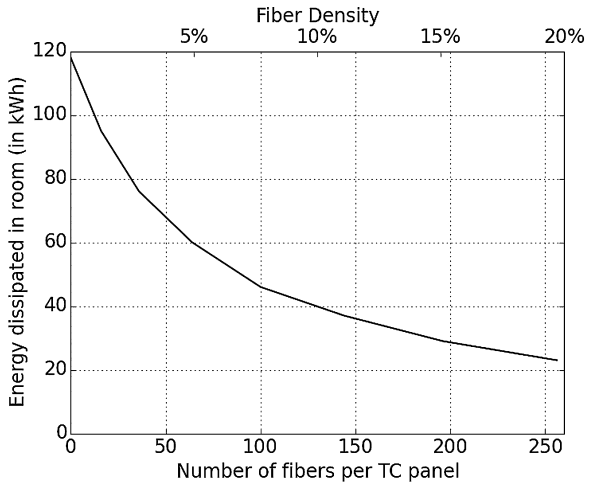

Fig. 16. Heat dissipated inside the room by fluorescent lamps for different volumetric ratios of optical fibers in the used TC panels.

The heat is dissipated inside the room from the use of artificial lighting and transmission of solar radiation for each day of the entire year. It is observed that for days when solar radiation into the room is low (due to presence of cloudy skies), more artificial illumination is necessitated which becomes the major reason for heat dissipation. On the contrary, the ratio of heat dissipated on weekends would be primarily attributed to the solar radiation into the room due to lower occupancy levels which requires lesser use of artificial lighting.

The cumulative heat dissipated due to electric lighting decreases as the volumetric ratio of optical fibers in the TC panels increases. This trend is observed in Fig. 16 where the utilization of fluorescent lamps reduces due to sufficient illumination present during longer times of the day. The rate of reduction in heat dissipation becomes more gradual as the number of fibers in the TC panels increases beyond 100 (~7.56% volumetric fiber density). This shows that the energy dissipated by lighting installations can never reach zero owing to random light-switching behavior of occupants.

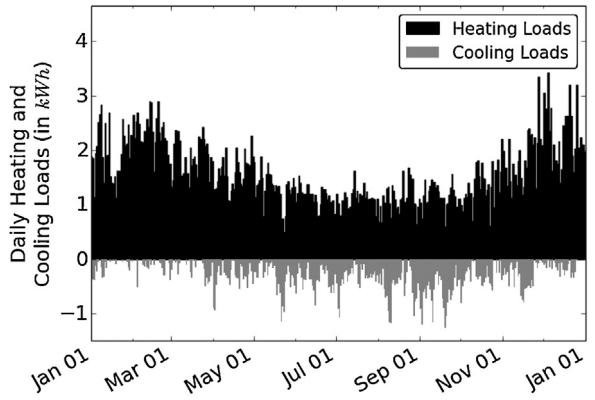

Fig. 17. The net daily heating and cooling loads experienced by the HVAC system due to conduction, heat dissipation by fluorescent tubes and solar radiation from optical fibers.

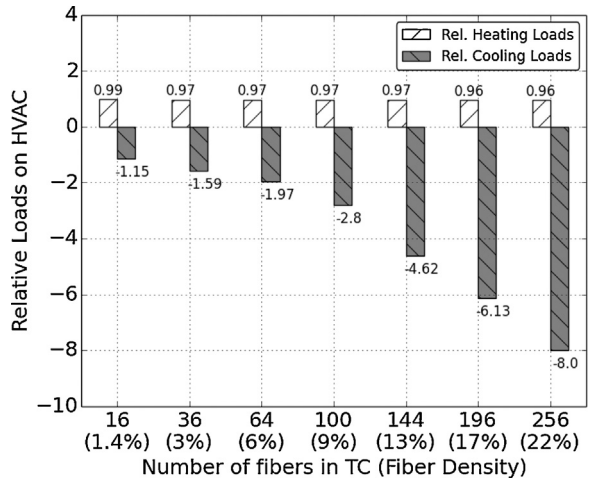

Fig. 18. Cumulative heating and cooling loads for a room with south-facing wall composed of TC panels compared to a south-facing opaque wall.

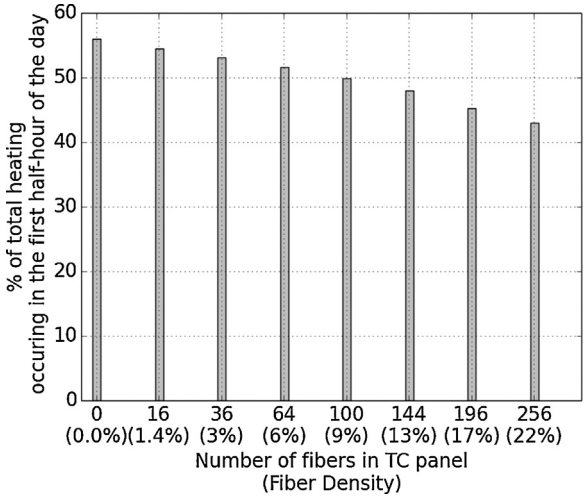

Fig. 19. The percentage of heat removed at the start of the day for the whole year to the total heat conducted away.

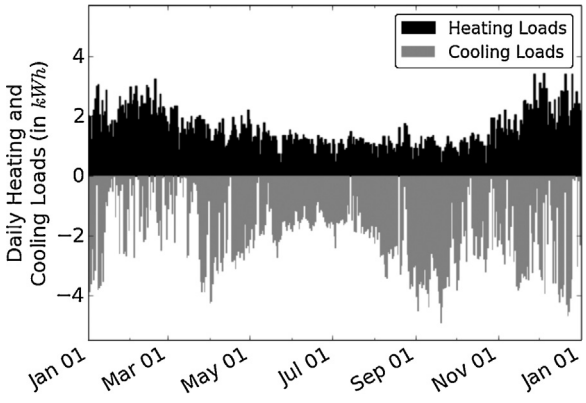

Fig. 20. Daily heating and cooling loads experienced by HVAC system in a room with TC panels containing 256 fibers.

Finally, the contribution of heat conduction through the walls is also considered which gives the total load on the HVAC system when combined with the loads due to solar radiation and heat dissipation due to artificial lighting. The initial temperature of the walls before the start of simulation (*i. e.* at 8 am) is set to the outside temperature for the previous hour (*i. e.* at 7 am). The parameters used in boundary conditions (*e. g.* wind speed (v_s), T_{amb}, q_{solar}, *etc.*) are first set at the start of the simulation and are then updated after every thirty minutes (by referring to the weather file for that time of the day).[1] The HVAC system is stopped at 6 pm, marking the end of the simulation period for the day. The simulations are repeated for all the days in the year to give the cumulative amount of heating and cooling loads on the HVAC system. Fig. 17 shows the distribution of net daily heating or cooling loads experienced by the room. Fig. 18 gives the relative variations in cumulative heating and cooling loads, for a room with a south-facing wall made up of TC panels with different optical fiber densities, when compared with a room with an opaque south-facing wall. Surprisingly, it is the observed from Fig. 18 that the heating loads are almost unchanged as the fiber density ratio in TC panels is increased. This can be attributed to three reasons: (1) The initial temperature of the walls at the start of the day is set to an ambient temperature at 7 *am*. Therefore, the majority of heating for the day is provided during the first half-hour (8 am–8:30 am) (Fig. 19), (2) during the morning times the solar radiation transmitted through the optical fibers is low which is not sufficient to equalize the heat loss through walls, and (3) the *R*-value of an optical fiber is about 2.81 times lower than the remaining wall structure. As the fiber volumetric ratio is increased, the heat in the room is further removed by conduction through the optical fibers. Thus, a slight reduction in the percentage of heat removed due to conduction at start of day for the entire year to the total heat conducted away is observed (Fig. 19). On the contrary, higher optical fiber density also causes overheating of the room, especially during winter afternoons when the Sun's altitude is low and almost normal to the wall, which imposes greater cooling loads and unfortunately, requires operating an air conditioning system even during winter months. This trend is shown in Fig. 20 for a room containing TC panels embedded with 256 fibers corresponding to 22.3% fiber volumetric ratio. The contributions of heat flow into the room separately due to conduction, solar radiation and heat dissipation from luminaires are given in Fig. 21. The positive values in Fig. 21 refers to the amount of heat gained by the room due to sources like solar radiation, *etc*. while negative values signify heat lost due to conduction through walls.

The energy that is spent by the HVAC to maintain a temperature of 22 °C inside the room can be monetized to give an estimate of the changes in expenditure on utilities due to the introduction of wall composed of TC panels. As an example case, consider an

[1] The half-hourly values are calculated from the weather file by taking the mean values of the parameters for the current hour and the next hour.

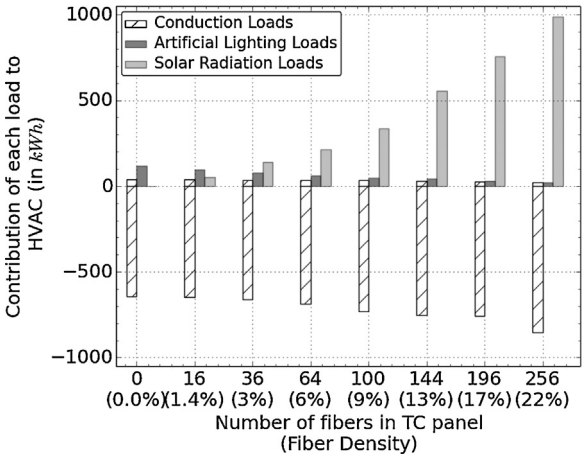

Fig. 21. The contribution of each of the heating and cooling loads (expressed in kWh) to the total HVAC load.

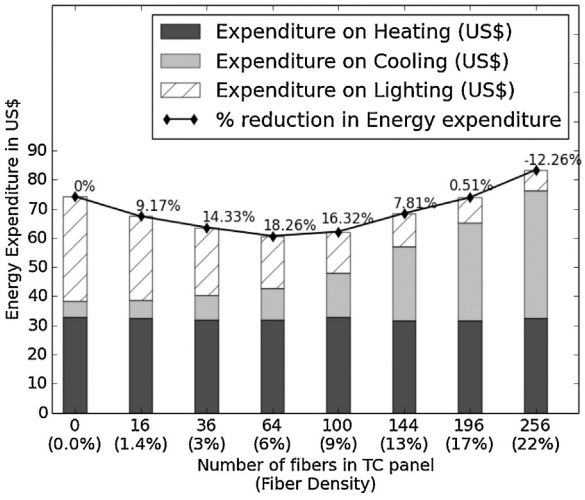

Fig. 22. Total expenditure on cooling, heating and lighting the room space; savings in energy due to replacement of a south-facing opaque wall with a wall made of TC panels.

HVAC system with a high efficiency gas furnace with 95% efficiency and an air conditioner with a Coefficient of Performance (COP) of 4.0. Also, in the San Francisco Bay Area on average, building owners pay 23.3 ¢/kWh for electricity and 5.4 ¢/kWh towards natural gas[2]. The expenditure on utilities for a room such as that shown in Fig. 14 with a south-facing wall composed of TC panels is normalized against the energy expenditure for a room having only opaque walls. The results from comparisons are shown in Fig. 22 which signifies the initial reduction of expenditure on energy which subsequently increases as the volumetric ratio of fibers increases. Thus, for a given COP of HVAC system and price per unit of electricity and natural gas, we can estimate the density of fibers in the TC panel to be 5.59% (64 fibers per panel) that will optimize the energy expenditure of a building.

A new building material called the ultra-lightweight cement composites (ULCC) has been developed in Wu et al. [25]. The material achieves its light weight from the inclusion of cenospheres that are typically hollow inert spheres produced as a byproduct of coal combustion. At the same time, the high structural strength needed to support the loads in a building is also maintained. For a complete overview of the different types of ULCC mixtures, the reader is referred to research published in Wu et al. [25]. In this example, we select the material properties (Table 2) for one type of ULCC mix referred to as 'ULCC-1' in Wu et al. [25]. With the inclusion of cenospheres, the thermal conductivity, λ_{ULCC} and the density, ρ_{ULCC} of the ULCC is lowered while the value of the specific heat, c_{ULCC} is slightly increased. The cenospheres provide a large interface area that increases slippage and act as a barrier to heat transfer which reduces the thermal conductivity of the mixture. In a TC panel, the concrete layer is replaced by a layer of ULCC and a new set of simulations for conduction calculations are implemented. The results in Fig. 23 show the expenditure on heating and cooling and the relative reduction in expenses after addition of cenospheres to the mix. Interestingly, the expenses for heating do not change since most of the heating is required during morning when the entire wall is below the comfort temperature of 22 °C. The redesigning of walls with ULCC prevents the loss of heat to the ambient environment but is rather ineffective during the morning as heat is lost from the steep temperature gradient existing between the drywall, XPS and ULCC, and the indoor air. The expenses for cooling, on the other hand, are reduced by about 6–20% depending on the density of optical fibers in the ULCC. As a result, for the given COP values of HVAC and price per unit of electricity and natural gas, a fiber density in the TC panel of 5.59% (64 fibers per panel) in ULCC panels can save approximately 20.5% of energy expenses compared to a room with opaque walls constructed from NWC.

Table 2
Material properties for ULCC and new wall composition.

Parameter	Value
External walls	ULCC (0.1 m), XPS insulation (0.075 m), Drywall (0.0156 m)
ULCC composition	Water, binder, cenospheres, superplasticizer, shrinkage reducing admixture
R-value of layered-wall	2.99 m^2 K/W
λ_{ULCC}	0.40 W/mK [25]
ρ_{ULCC}	1303 kg/m^3 [25]
$c_{p,ULCC}$	788 J/kg K [4]

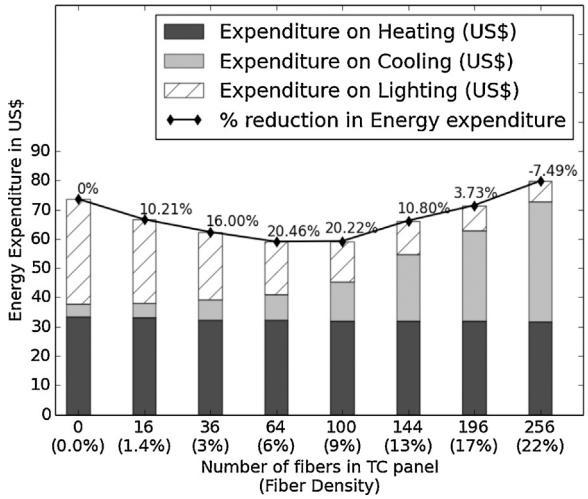

Fig. 23. Total expenditure on cooling, heating and lighting the room space; estimated savings in energy after redesigning the TC panels and walls with ULCC and comparing the results with a room containing opaque walls constructed from NWC.

4. Conclusion

The research on a novel building construction material called translucent concrete (TC) has been presented in this study. The present-day softwares for analyzing building physics (*e. g.* *Energy-*

[2] Source: U.S. Bureau of Labor Statistics, http://www.bls.gov/regions/west/news-release/averageenergyprices_sanfrancisco.htm.

Plus) are limited to materials that are either opaque (*e. g*. walls or partitions) or transparent (*e. g*. windows). Hence, it became necessary as part of this research to develop a software that could model and simulate a translucent system which inculcated the hybrid features of both opaque regions and transparent light-channeling components. The software estimated the heating and cooling loads experienced by the HVAC system of a room due to the solar radiation input from the optical fibers, the conduction through the walls and the heat dissipated from artificial lighting. The solar radiation calculations followed from geometrical ray tracing, the heat dissipated by the use of fluorescent tubes employed lighting schedules derived from occupancy profiles and heat conduction was computed using finite difference methods applied to walls with boundary conditions derived from the TMY weather file for Berkeley (California). It was observed that solar radiation through optical fibers imposed large cooling loads on the HVAC system for large fiber volumetric ratios in the TC panels. Further, higher fiber ratios provided sufficient daylight illumination for greater part of the year which helped in curtailing heat dissipated by lighting installations and in general, saved lighting energy. The conduction through the layered wall removed a significant amount of heat during the morning which necessitated the usage of heating during those times. From calculations, it became clear that a fiber volumetric ratio of around 6% in a south-facing TC wall was best suited to reduce the overall energy usage by about 18% compared to a completely sunlight-deprived room. The use of materials that have lower conductivity values like the ULCC, instead of NWC, improved the total R-value of the walls and saved another approximately 2% energy utilization over the duration of the entire year.

The use of lower fiber density also supports the construction procedure of TC panels since optical fibers constitute the most expensive component in the entire mix in terms of material costs. Moreover, construction costs are a function of the number of fibers that have to be laid parallel to each other in the formwork. The use of low fiber density also generates less stress concentration regions in concrete that might eventually lead to the fracture of the TC panel. As a result, a fiber density of ~6% would be reasonable in containing the costs of the TC panel while functioning as an innovative energy saving building material for the façade. The results presented in Figs. 22 and 23 are based on commonly used values for COP of an air conditioner and gas furnace efficiency. It is seen that the savings in energy expenditure fluctuates greatly as the COP of the HVAC equipment changes. Thus, it is important that for a place like Berkeley, only high efficiency air conditioners and gas furnaces are used to maximize the reduction in expenditure over time.

Funding

The presented research is funded by the Republic of Singapore's National Research Foundation through a grant to the Berkeley Education Alliance for Research in Singapore (BEARS) for Singapore-Berkeley Building Efficiency and Sustainability in the Tropics (SinBerBEST) Program. BEARS has been established by the University of California, Berkeley as a center for intellectual excellence in research and education in Singapore.

Conflict of interest

No potential conflict of interest was reported by the authors.

Acknowledgements

The authors would like to thank the students and staff in CREST, Cory Hall, Berkeley, CA for their cooperation in providing the sensor data. The authors would like to thank Dr. Kemal Celik and Alex R. Mead for conducting illuminance experiments in the testbed room and sharing light distribution data. The authors would like to thank the staff at Solar Energy Research Institute of Singapore (SERIS) for their assistance in measuring the physical properties of the TC panels.

Appendix A.

Geometrical ray theory

The theory for Ray Tracing is formulated using the Eikonal equation for wavefront of light. The Eikonal equation is discretized spatially and time is updated to represent the marching of rays in space. The formulation of a ray of light using Eikonal equation is given as

$$\frac{d(n\hat{\mathbf{s}})}{ds} = \nabla n \tag{22}$$

where $n(x, y, z)$ is the refractive index of the medium at a space coordinate (x, y, z) and the direction of light ray is given by the unit vector, $\hat{\mathbf{s}}$. Let $\hat{\mathbf{s}}$ be described in terms of its direction cosines, $[\cos\alpha, \cos\beta, \cos\gamma]$, with $[\alpha, \beta, \gamma]$ being the angles between the direction of ray path and $[x, y, z]$ axes, respectively. Differentiating left hand expression in Eq. (22) gives:

$$n\frac{d\hat{\mathbf{s}}}{ds} = \nabla n - \hat{\mathbf{s}}\frac{dn}{ds} \tag{23}$$

The directional derivative of dn/ds in direction $\hat{s}$ is written as

$$\frac{dn}{ds} = \hat{\mathbf{s}}.\nabla n \tag{24}$$

Combining Eqs. (23) and (24) and rearranging the terms give

$$\frac{d\hat{\mathbf{s}}}{ds} = \frac{1}{n}(\nabla n - (\hat{\mathbf{s}}.\nabla n)\hat{\mathbf{s}}) \tag{25}$$

where

$$\nabla n = \left[\frac{\partial n}{\partial x}, \frac{\partial n}{\partial y}, \frac{\partial n}{\partial z}\right] = [n_x, n_y, n_z] \tag{26}$$

Eq. (25) is separated into components which are written as:

$$\frac{d(\cos\alpha)}{ds} = \frac{1}{n}\left\{n_x - \left(\nabla n.\hat{\mathbf{s}}\right)\cos\alpha\right\} \tag{27}$$

$$\frac{d(\cos\beta)}{ds} = \frac{1}{n}\left\{n_y - \left(\nabla n.\hat{\mathbf{s}}\right)\cos\beta\right\} \tag{28}$$

$$\frac{d(\cos\gamma)}{ds} = \frac{1}{n}\left\{n_y - \left(\nabla n.\hat{\mathbf{s}}\right)\cos\gamma\right\} \tag{29}$$

To integrate Eqs. (27), (28) and (29), the forward Euler scheme is used. The equations are discretized along the path length, ds, to give:

$$d(\cos\alpha) \rightarrow (\cos\alpha)_{k+1} - (\cos\alpha)_k \tag{30}$$

$$d(\cos\beta) \rightarrow (\cos\beta)_{k+1} - (\cos\beta)_k \tag{31}$$

$$d(\cos\gamma) \rightarrow (\cos\gamma)_{k+1} - (\cos\gamma)_k \tag{32}$$

$$ds \rightarrow \Delta s \tag{33}$$

where k denotes the integration step, and Δs is a finite integration step. The discretized form is expressed as

$$(\cos\alpha)_{k+1} = \frac{1}{n}\left\{n_x - \left(\nabla n.\hat{\mathbf{s}}\right)\cos\alpha\right\}_k \Delta s + (\cos\alpha)_k \tag{34}$$

$$(\cos\beta)_{k+1} = \frac{1}{n}\left\{n_y - \left(\nabla n.\hat{\mathbf{s}}\right)\cos\beta\right\}_k \Delta s + (\cos\beta)_k \tag{35}$$

and to determine $(\cos\gamma)_{k+1}$, the property of directional cosines can be used:

$$(\cos\gamma)_{k+1} = \sqrt{1 - (\cos\alpha)_{k+1}^2 - (\cos\beta)_{k+1}^2} \tag{36}$$

Finally, the ray position at any instant can be expressed in the following form:

$$x_{k+1} = x_k + \Delta s(\cos\alpha)_{k+1} \tag{37}$$

$$y_{k+1} = y_k + \Delta s(\cos\beta)_{k+1} \tag{38}$$

$$z_{k+1} = z_k + \Delta s(\cos\gamma)_{k+1} \tag{39}$$

Thus, the time spent by light ray in the optical system is evaluated as:

$$T_{k+1} = T_k + \frac{\Delta s}{u} = T_k + \frac{\Delta s}{c/n} \tag{40}$$

where u is the wave speed in the medium of propagation and c is the absolute speed of light in vacuum. Note that $n = \frac{u}{c}$.

Remark: The travel times of different light rays calculated using the discretization presented above can also be used to assess the dispersion properties of the optical medium.

The value of ∇n can be estimated using finite differences as follows:

$$\begin{aligned}\nabla n &= [n_x, n_y, n_z] \\ &= \left[\frac{n(x+\delta x, y, z) - n(x, y, z)}{\delta x}, \frac{n(x, y+\delta y, z) - n(x, y, z)}{\delta y}, \right. \\ &\quad \left. \frac{n(x, y, z+\delta z) - n(x, y, z)}{\delta z}\right]\end{aligned} \tag{41}$$

The values of $[\delta x, \delta y, \delta z]$ are chosen to be very small, usually an order of magnitude smaller than the value chosen for Δs.

References

[1] A. Ahuja, K.M. Mosalam, T.I. Zohdi, Computational modeling of translucent concrete panels, J. Archit. Eng. 21 (2014) B4014008.
[2] A. Ahuja, K.M. Mosalam, T.I. Zohdi, An illumination model for translucent concrete using RADIANCE, in: 14th International Conference of the International Building Performance Simulation Association (IBPSA), Hyderabad, India, 2015, pp. 2579–2586.
[3] P.R. Boyce, J.A. Veitch, G.R. Newsham, C.C. Jones, J. Heerwagen, M. Myer, C.M. Hunter, Occupant use of switching and dimming controls in offices, Light. Res. Technol. 38 (4) (2006) 358–376.
[4] D.D.L. Chung, Cement-matrix composites for thermal engineering, Appl. Thermal Eng. 21 (16) (2001) 1607–1619.
[5] M.P. Gutierrez, T.I. Zohdi, Effective reflectivity and heat generation in sucrose and PMMA mixtures, Energy Build. 71 (2014) 95–103.
[6] D.R.G. Hunt, The use of artificial lighting in relation to daylight levels and occupancy, Build. Environ. 14 (1) (1979) 21–33.
[7] T. Ishigure, E. Nihei, Y. Koike, Optimum refractive-index profile of the graded-index polymer optical fiber, toward gigabit data links, Appl. Opt. 35 (12) (1996) 2048–2053.
[8] W. Jones, Linear optical properties of organic solids, in: Organic Molecular Solids: Properties and Applications, CRC Press, 1997.
[9] T. Kaino, Absorption losses of low loss plastic optical fibers, Jpn. J. Appl. Phys. 24 (12R) (1985).
[10] D. Kato, T. Nakamura, Application of optical fibers to the transmission of solar radiation, J. Appl. Phys. 47 (10) (1976) 4528–4531.
[11] D. Lindelöf, N. Morel, A field investigation of the intermediate light switching by users, Energy Build. 38 (7) (2006) 790–801.
[12] X. Liu, W. Cai, W. Lei, X. Du, W. Chen, Far-field distance for surface light source with different luminous area, Appl. Opt. 52 (8) (2013) 1629–1635.
[13] J.A. Love, Manual switching patterns in private offices, Light. Res. Technol. 30 (1) (1998) 45–50.
[14] W. Lu, B. Huang, S. Chen, K.M. Mosalam, Shaking table test method of building curtain walls using floor capacity demand spectrum, Bull. Earthq. Eng. (2016).
[15] W. Lu, B. Huang, K.M. Mosalam, S. Chen, Experimental evaluation of a glass curtain wall of a tall building, Earthq. Eng. Struct. Dyn. 45 (7) (2016) 1185–1205.
[16] S.L. Manzello, S.H. Park, T. Mizukami, D.P. Bentz, Measurement of thermal properties of gypsum board at elevated temperatures, in: Proceedings of the 5th International Conference on Structures in Fire, Nanyang Technological University, Singapore, 2008, pp. 656–665.
[17] W.H. McAdams, Heat Transmission, 3rd ed, McGraw-Hill Kogakusha, Tokyo, Japan, 1954.
[18] J. Page, D. Robinson, N. Morel, J.L. Scartezzini, A generalised stochastic model for the simulation of occupant presence, Energy Build. 40 (2) (2008) 83–98.
[19] R. Perez, R. Seals, P. Ineichen, R. Stewart, D. Menicucci, A new simplified version of the Perez diffuse irradiance model for tilted surfaces, Solar Energy 39 (3) (1987) 221–231.
[20] S. Pigg, M. Eilers, J. Reed, Behavioural aspects of lighting and occupancy sensors in privates offices: a case study of a university office building, Proceedings of ACEEE Summer Study on Energy Efficiency in Buildings, vol. 8 (1996) 161–171.
[21] M. Praprotnik, M. Sterk, R. Trobec, Inhomogeneous heat-conduction problems solved by a new explicit finite difference scheme, Int. J. Pure Appl. Math. 13 (3) (2004) 275–291.
[22] Y. Qin, D. Lin, S.Y. Hui, A simple method for comparative study on the thermal performance of LEDs and fluorescent lamps, IEEE Transactions Power Electronics, vol. 24 (2009) 1811–1818.
[23] C.F. Reinhart, K. Voss, Monitoring manual control of electric lighting and blinds, Light. Res. Technol. 35 (3) (2003) 243–260.
[24] O. Seppänen, W.J. Fisk, Q.H. Lei, Effect of Temperature on Task Performance in Offfice Environment. Technical report, Lawrence Berkeley National Laboratory, Berkeley, CA, 2006.
[25] Y. Wu, J.Y. Wang, P.J. Monteiro, M.H. Zhang, Development of ultra-lightweight cement composites with low thermal conductivity and high specific strength for energy efficient buildings, Constr. Build. Mater. 87 (2015) 100–112.
[26] T.I. Zohdi, Modeling and simulation of the optical response rod-functionalized reflective surfaces, Comput. Mech. 50 (2) (2012) 257–268.
[27] J. Zubia, J. Arrue, Plastic optical fibers: an introduction to their technological processes and applications, Opt. Fiber Technol. 7 (2) (2001) 101–140.